Effects of Angiopoietin-2-Blocking Antibody on Endothelial Cell–Cell Junctions and Lung Metastasis

DOI: 10.1093/jnci/djs009
Advance Access publication on February 17, 2012.

ARTICLE

Effects of Angiopoietin-2-Blocking Antibody on Endothelial Cell–Cell Junctions and Lung Metastasis

Tanja Holopainen, Pipsa Saharinen, Gabriela D'Amico, Anita Lampinen, Lauri Eklund, Raija Sormunen, Andrey Anisimov, Georgia Zarkada, Marja Lohela, Hanna Heloterä, Tuomas Tammela, Laura E. Benjamin, Seppo Ylä-Herttuala, Ching Ching Leow, Gou Young Koh, Kari Alitalo

Manuscript received May 2, 2011; revised January 5, 2012; accepted January 5, 2012.

Correspondence to: Kari Alitalo, MD, PhD, Molecular/Cancer Biology Laboratory, Biomedicum Helsinki, Haartmaninkatu 8 (PO Box 63), FI-00014 University of Helsinki, Helsinki, Finland (e-mail: kari.alitalo@helsinki.fi).

Background Angiopoietin-2 (Ang2), a ligand for endothelial TEK (Tie2) tyrosine kinase receptor, is induced in hypoxic endothelial cells of tumors, where it promotes tumor angiogenesis and growth. However, the effects of Ang2 on tumor lymphangiogenesis and metastasis are poorly characterized.

Methods We addressed the effect of Ang2 on tumor progression and metastasis using systemic Ang2 overexpression in mice carrying tumor xenografts, endothelium-specific overexpression of Ang2 in VEC-tTA/Tet-OS-Ang2 transgenic mice implanted with isogenic tumors, and administration of Ang2-blocking antibodies to tumor-bearing immunodeficient mice. Fisher's exact test was used for analysis of metastasis occurrence, and repeated measures one-way analysis of variance was used for the analysis of primary tumor growth curves. Unpaired *t* test was used for all other analyses. All statistical tests were two-sided.

Results Adenoviral expression of Ang2 increased lymph node and lung metastasis in tumor xenografts. The metastatic burden in the lungs was increased in transgenic mice in which Ang2 expression was induced specifically in the vascular endothelium (tumor burden per grid, VEC-tTA/Tet-OS-Ang2 mice [n = 5] vs control mice [n = 4]: 45.23 vs 12.26 mm^2, difference = 32.67 mm^2, 95% confidence interval = 31.87 to 34.07, $P < .001$). Ang2-blocking antibodies reduced lymph node and lung metastasis, as well as tumor lymphangiogenesis, and decreased tumor cell homing to the lungs after intravenous injection. In the lung metastases, Ang2 overexpression decreased endothelial integrity, whereas the Ang2-blocking antibodies improved endothelial cell–cell junctions and basement membrane contacts of metastasis-associated lung capillaries. At the cellular level, the Ang2-blocking antibodies induced the internalization of Ang2-Tie2 receptor complexes from endothelial cell–cell junctions in endothelial–tumor cell cocultures.

Conclusion Our results indicate that blocking Ang2 inhibits metastatic dissemination in part by enhancing the integrity of endothelial cell–cell junctions.

J Natl Cancer Inst 2012;104:461–475

Angiopoietins (Ang, also known as Angpt), ligands of the endothelial TEK (Tie2) tyrosine kinase receptor, have been associated with vascular remodeling and stabilization signals in angiogenesis (1,2). In the blood vascular endothelium, Ang1 exerts agonistic functions via increased phoshorylation of Tie2 (3). Both Ang1 and Tie2 are essential for the remodeling of a functional blood vessel network during embryogenesis (4–6). They also promote various functions characteristic of the mature blood vasculature, such as endothelial cell survival (7). Until very recently, Ang2 was considered primarily as a Tie2 antagonist, being expressed mainly at sites of vascular remodeling where it destabilizes the vascular endothelium (8). However, evidence is emerging that Ang2 may have different roles in the vasculature depending on the context (9,10). The antagonistic function of Ang2 is required for normal development of retinal vessels during ocular angiogenesis (11), whereas its Tie2 agonist activity is required for normal lymphatic vascular development (12).

Ang2 expression is increased in activated and hypoxic vascular endothelial cells in tumors, where it acts as an Ang1 antagonist and promotes tumor angiogenesis and growth (13–16). Nasarre et al. (17) described an initial transient inhibition of tumor growth and angiogenesis in mice with genetically ablated Ang2 (17). The blockade of Ang2 with antibodies and peptide-Fc fusion proteins results in suppression of primary tumor growth and angiogenesis (16,18,19). Notably, elevated circulating Ang2 in patients with pancreatic ductal adenocarcinoma was associated with the extent of lymphatic metastasis (20). However, very little is known about the effects of Ang2 inhibition on metastasis. Because the formation of metastases is often crucial for the prognosis of patients, it is important to evaluate the effect of Ang2 targeting on tumor cell dissemination and the development of metastases. Thus, we investigated the effect of Ang2 on tumor progression and metastasis using several different model systems.

CONTEXTS AND CAVEATS

Prior knowledge

Angiopoietins (Ang) are ligands of the Tie2 tyrosine kinase receptor and function in vascular remodeling during embryogenesis. Ang2 is also overexpressed in hypoxic vascular endothelial cells in tumors and promotes tumor angiogenesis and growth. However, the mechanisms of Ang2 action in tumor progression and metastasis are poorly known.

Study design

The effects of Ang2 on angiogenesis, tumor growth, and metastasis in lungs were studied by systemic and endothelial cell–specific Ang2 overexpression in mice carrying tumor xenografts and in transgenic mice implanted with isogenic tumors. The effect of Ang2 inhibition was studied with anti-Ang2 antibodies in tumor-bearing immunodeficient mice.

Contribution

Ang2 increased tumor metastasis at least in part by promoting endothelial disruption and increasing tumor cell translocation and homing to target organs. Ang2 inhibition also attenuated tumor lymphangiogenesis, dissemination of tumor cells via the lymphatic vessels, and tumor cell colonization of the lungs.

Implication

Ang2 may promote metastasis in part by disrupting the integrity of endothelial cell–cell junctions.

Limitations

Rapidly growing tumors were used in the models. The dose–response range was not evaluated, and because of the rapid tumor growth and treatment schedules, possible adverse effects related to the treatment may have gone unnoticed. It remains to be investigated if the Ang2 antibodies can inhibit metastatic colonization of other tissues besides the lungs.

From the Editors

Methods

Mice

Six- to eight-week-old female severe combined immunodeficient (SCID) and nu/nu BALB/c mice were obtained from Harlan Laboratories (Venray, The Netherlands) and 8- to 12-week-old NOD SCID gamma (NSG) mice (stock no. 005557) were obtained from the Jackson Laboratory (Bar Harbor, ME). VEC-tTA/Tet-OS-Ang2 transgenic mice and their littermate controls were used in the experiments. The TET-OS-Ang2 responder construct was made by polymerase chain reaction cloning of the full-length mouse Ang2 open reading frame using the cDNA (GenBank NW_001030882.1) downstream of the TET-responsive promoter in the pTET-OS-vector [described in (21,22) and Supplementary Tables 1 and 2, available online]. Transgenic mouse lines were generated by injection of the 2.7-kb expression cassette from the vector into fertilized mouse oocytes of the strain FVB/NIH. The driver VE-cadherin-tTA [VEC-tTA, (23)] and responder transgenic mouse lines were bred together to obtain double transgenic VEC-tTA/Tet-OS-Ang2 offspring. To overcome the embryonic lethality attributable to endothelial Ang2 overexpression in double transgenic embryos [(8) and our unpublished data], Ang2 expression was repressed during the entire pregnancy. Tetracycline (Sigma-Aldrich, St Louis, MO) at 2.0 mg/mL in 5% sucrose was added to the drinking water of pregnant females, starting at the time of mating and until birth, when Ang2 expression was induced by discontinuation of tetracycline administration. Single transgenic or wild-type littermates were used as controls for double transgenic mice. None of the control mice displayed any obvious phenotype. The National Board for Animal Experiments at the Provincial State Office of Southern Finland approved all experiments, which were performed in accordance with the Finnish legislation regarding the humane care and use of laboratory animals.

Cell Culture

The human lung cancer cell line NCI-H460-LNM35 (hereafter LNM35) is the previously used and characterized luciferase-tagged subline of NCI-H460-N15, a human non–small cell carcinoma of the lung (24); Lewis lung carcinoma (LLC) and HeLa cells were purchased from the American Type Culture Collection (ATCC, Manassas, VA) and luciferase-tagged B16-F10 melanoma cells were obtained from Caliper Life Sciences Inc (Hopkinton, MA) (used in passages below 30). LNM35 cells were maintained in RPMI-1640 medium supplemented with 2 mM L-glutamine, penicillin (100 U/mL), streptomycin (100 μg/mL), and 10% fetal calf serum (PromoCell, Heidelberg, Germany). LLC, HeLa, and luciferase-tagged B16-F10 melanoma cells were maintained in Dulbecco's Modified Eagle's Medium (DMEM) supplemented with 2 mM L-glutamine, penicillin (100 U/mL), streptomycin (100 μg/mL), and 10% fetal calf serum (PromoCell). Human dermal microvascular lymphatic endothelial cells (LECs) and blood microvascular endothelial cells (BECs) (PromoCell) were maintained on fibronectin-coated dishes in Endothelial Cell Basal Medium MV (ECBM; PromoCell) with growth supplements provided by the manufacturer and used in passages 2–6. Vascular endothelial growth factor-C [100 ng/mL, (25)] was added to the LEC growth medium. For stimulation, 200 ng/μL COMP-Ang1 [Cartilage oligomeric matrix protein-Ang1, (26)] was added to the endothelial cells for 30 minutes.

Antibody Inhibition of Tumor Growth

Luciferase-tagged LNM35 tumor cells (5×10^6 cells per mouse) were implanted into SCID or nu/nu BALB/c mice anesthetized with ketamine (Ketaminol; Orion Pharma, Espoo, Finland; or Ketalar; Pfizer, New York, NY) and xylazine (Rompun et; Bayer Healthcare, Leverkusen, Germany). Once the primary tumor volumes reached 150–200 mm^3, the mice (n = 8–10 per group) were randomly assigned to receive an intraperitoneal injection of the Ang2-blocking antibody [MEDI3617; MedImmune, Gaithersburg, MD; (27)] at a dose of 10 mg/kg, or an equal dose of control human immunoglobulin G (hIgG). Thereafter, the intraperitoneal administration of the antibodies and tumor diameter measurements were repeated every second day. At day 16, the primary tumors and inguinal regional lymph nodes were excised, weighed, imaged for bioluminescence, measured in three dimensions with a digital caliper, photographed, and processed for histological analysis.

Tumor Assays Using AdAng2

Luciferase-tagged LNM35 cells were implanted subcutaneously into female SCID mice (n = 9–10 per group), followed by intravenous

administration of recombinant in vitro tested AdAng2 (28) or AdLacZ, and the primary tumor growth was analyzed as described above. At 14 days, D-luciferin (Synchem, Felsberg, Germany) was administered intraperitoneally at the dose of 150 mg/kg, followed by imaging for bioluminescence 10 minutes after injection. Photonic signal intensities were quantified using the Living Image software (Xenogen Corporation, Alameda, CA). At 3 weeks, the primary tumors and the lymph nodes were excised, imaged for bioluminescence, weighed, measured for volume with a digital caliper, and processed for histology.

To evaluate lung metastasis, SCID mice (n = 3–6 per group) were killed at 4 weeks after the removal of the primary tumors at 3 weeks, and the lungs were weighed and their bioluminescence signal was measured. The bioluminescent signal intensity emitted from the metastatic foci was quantified with Living Image Software (Xenogen Corporation). The area of region of interest was kept constant for all the samples.

Lung Colonization Experiments

SCID or NSG mice (n = 4 in each group) were injected intravenously with adenoviruses encoding angiopoietin-2 (AdAng2) or β-galactosidase (AdLacZ) 2 days before systemic inoculation of green fluorescent protein (GFP)–tagged LNM35 cells, and lung colonization was analyzed 4 days thereafter with fluorescent microscopy. To evaluate metastatic growth at later time points, B16-F10 or LNM35 cells were implanted intravenously into AdAng2- and AdLacZ-treated mice, and the lungs were excised at 2 (B16-F10) or 3 (LNM35) weeks, weighed, imaged under a microscope, and processed for histology. Ang2-blocking antibody (10 mg/kg) or an equal amount of hIgG were administered intravenously into the mice every second day starting at 4 days before systemic injection of the GFP- or luciferase-tagged LNM35 cells. The lungs of the mice injected with fluorescently tagged tumor cells were analyzed 8 days after tumor cell inoculation by microscopy (Leica MZFLIII, Leica Microsystems, Vienna, Austria). The homing of luciferase-positive LNM35 tumor cells into the lungs of mice treated with Ang2-blocking antibodies or hIgG was evaluated by bioluminescence imaging ex vivo at 5 days. The extent of lung colonization of systemically administered B16-F10 cells in Ang2-blocking antibody vs hIgG-treated mice was assessed at 2 weeks, as described above.

In experiments using the inducible transgenic mouse model, B16-F10 melanoma cells (1×10^5 cells) were inoculated intravenously into the conditionally transgenic Ang2 mice and their littermate controls, and the lungs were analyzed 3 weeks after the implantation.

Transmission Electron Microscopy

Lung specimens containing melanoma cell colonies from Ang2-overexpressing, wild-type C57Bl/6J, Ang2-blocking antibody-treated, and human serum albumin (HSA) control NSG mice (three mice per group) were fixed in 1% glutaraldehyde and 4% formaldehyde in 0.1 M phosphate buffer, pH 7.4, postfixed in 1% osmium tetroxide, dehydrated in acetone, and embedded in Epon LX112 (Ladd Research Industries, Williston, VT). Sections of 1.0 μm were stained with toluidine blue for histological analysis, and 80-nm sections were cut with a Leica Ultracut UCT microtome (Leica Microsystems, Vienna, Austria) At least three specimens from each mouse were examined using a Philips CM100 transmission electron microscope. Metastasis-associated capillaries, the extent of endothelial cell attachment from the basement membrane, and the morphology of endothelial cell–cell junctions were assessed and quantified from the samples. Images were captured with a Morada CCD camera (Olympus Soft Imaging Solutions GMBH, Munster, Germany).

Retinal Angiogenesis Assay

For the retina experiments, the Naval Medical Research Institute (NMRI) pups (n = 3–4 per group) were subcutaneously injected with 30 mg/kg of Ang2-blocking antibody or hIgG during postnatal day (P)0–P4, killed on P5, and the eyes were collected for analysis. Blood vessels in the retinas were visualized using biotinylated Griffonia simplicifolia lectin (Vector Laboratories, Burlingame, CA), followed by immunostaining. The following primary antibodies were used: rat anti-mouse Tie2 (TEK4; eBiosciences, San Diego, CA; 1:200) and rabbit anti-mouse neural/glial antigen 2 (NG2, MAB5384; Millipore, Billerica, MA; 1:1000). The primary antibodies were detected with the appropriate Alexa secondary antibody conjugates (Molecular Probes, Invitrogen, Carlsbad, CA). The samples were analyzed with a confocal microscope (Zeiss LSM 5 Duo (Carl Zeiss AG, Oberkochen, Germany), objectives ×10 with NA 0.45, oil objectives ×40 with NA 1.3 and ×63 with NA 1.4) by using multichannel scanning in frame mode. The pinhole diameter was set at one Airy unit for detection of the Alexa 488 signal and was adjusted for identical optical slice thickness for the fluorochromes emitting at higher wavelengths. Three-dimensional projections were digitally reconstructed from confocal z-stacks. Colocalization of signals was assessed from single confocal optical sections. Images of whole retinas were acquired using tile scanning using a pinhole diameter greater than three Airy units.

Immunohistochemical Staining

Five-to seven-micrometer sections of paraffin-embedded tissue or frozen sections were immunostained with monoclonal antibodies against platelet endothelial cell adhesion molecule 1[PECAM-1, also known as cluster of differentiation 31 (CD31); BD Biosciences, San Diego, CA; dilution 1:500], lymphatic vessel endothelial hyaluronan receptor-1 (LYVE-1) (29), neural/glial antigen 2 (NG-2; MAB5384; Millipore; dilution 1:300), or laminin (NeoMarkers, Fremont, CA; dilution 1:500). The occurrence of metastatic LNM35 foci in lymph nodes was detected using anti-cytokeratin 7 antibodies (Millipore; dilution 1:200). The primary antibodies were detected with the Tyramide Signal Amplification detection method (PerkinElmer Life Sciences, Waltham, MA) according to manufacturer instructions or using fluorescently conjugated secondary antibodies (Molecular Probes, Invitrogen; dilution 1:500 for 1 hour). Immunofluorescent staining to detect pimonidazole adducts was done with the HypoxyProbe-1 Plus Kit as instructed by the manufacturer (Natural Pharmacia International, Burlington, MA).

Cell Staining

All cells were fixed for 10 minutes in 4% paraformaldehyde (PFA) phosphate buffered saline (PBS), permeabilized 3 minutes with 0.1% Triton X-100 in PBS, blocked 5 minutes in 1% bovine

serum albumin (BSA) PBS, and incubated with primary antibodies against Tie1 (dilution 1:100), phosphorylated Tie2 (dilution 1:100), Tie2 (dilution 1:100) and Ang2 (dilution 1:50) (all from R&D Systems, Minneapolis, MN), VE-cadherin (BD Biosciences; dilution 1:100), phosphorylated endothelial nitric oxide synthase (pS1177; Cell Signaling Technology Inc, Danvers, MA; dilution 1:50), or a tight junction marker ZO-1 (Invitrogen; dilution 1:200), in 1% BSA PBS 30 minutes at room temperature. The cells were then incubated with secondary antibodies (Molecular Probes, Invitrogen; dilutions 1:300) 30 minutes at room temperature. All experiments were repeated at least twice with similar results.

Endothelial–Tumor Cell Coculture

BECs transfected with Tie2-GFP (30) retrovirus were cultured on fibronectin-coated Transwell filters (0.4 mm pore size) overnight, after which the filters were transferred to new 24-well plates with or without overnight cultures of LNM35 in the lower compartment (31). The cells were grown in endothelial cell medium for 48 hours in the presence or absence of the Ang2-blocking antibody (2 μg/mL), after which BECs were fixed and used for immunofluorescence staining.

Image Analysis

Bright field sections were viewed with a Leica DM LB microscope (Leica Microsystems GmbH, Wetzlar, Germany), and images were captured with a Penguin Pro 600es color camera (Pixera Corporation, Santa Clara, CA). Immunofluorescent images were captured with a Zeiss digital Axiocam camera connected to a Zeiss Axioplan 2 microscope (Carl Zeiss AG, Oberkochen, Germany). Confocal images were captured using laser scanning confocal microscopes Zeiss LSM 510 Meta, Zeiss LSM 5 Duo (Carl Zeiss AG), and Olympus FluorView FV1000 (Olympus, Tokyo, Japan).

At least five tumors were examined in each experimental group, and images from three distinct areas characterized by the mean representative density of vessels were captured from each tumor under evaluation. The image quantification was carried out using ImageJ software (The National Institutes of Health, Bethesda, MD).

Ang2 Small Interfering RNA (siRNA) Experiments

Sixty percent confluent overnight cultures of BECs expressing the previously characterized Tie2-GFP retrovirus vector (24) were transfected with siRNA targeted against human Ang2 (Santa Cruz, CA; sc-39305) or with control siRNA (Santa Cruz; sc-37007) using Oligofectamine (Invitrogen) and analyzed 48 hours later.

Analysis of Internalization of Cell Surface–Bound Anti-Ang2 antibody

LECs transfected with Tie2-GFP lentivirus were incubated in ECBM with anti-Ang2 antibody or control hIgG (2 μg/mL) on ice for 40 minutes following 30 minutes incubation on ice or at 37°C to induce the antibody uptake. Cells were either fixed with 4% PFA PBS or subjected to acid wash (2 mM glycine in Dulbecco, pH 2.0) for 15 minutes to remove the plasma membrane–bound antibodies and then fixed. For immunofluorescence staining, cells were permeabilized for 5 minutes with 0.1% Triton X-100 in PBS.

In Vitro Detection of Adenoviral Expression

To assess the expression of the adenoviral vector encoded constructs, HeLa cells were treated with DMEM starvation medium 30 minutes and transfected for 2 hours with adenoviruses expressing Ang2 (AdAng2) or ß-galactosidase (AdLacZ) (100 MOI). The cells were incubated in complete DMEM for 2 days, starved for 40 minutes in methionine- and cysteine-free Eagle's Minimum Essential Medium, and metabolically labeled in this medium supplemented with [^{35}S] methionine/[^{35}S]cysteine (Amersham Biosciences and GE Healthcare, Waukesha, WI) at 100 μCi/mL for 10 hours. Conditioned medium was then harvested and cleared of particulate material by centrifugation. Proteins were immunoprecipitated with a monoclonal antibody against the FLAG tag (Sigma-Aldrich; dilution 1:100) in the AdAng2 construct. The antigen–antibody complexes were incubated with protein G sepharose (Amersham Biosciences), subjected to sodium dodecyl sulfate–polyacrylamide (SDS–PAGE) gel electrophoresis and visualized with autoradiography.

Construction of Plasmids and Production of Recombinant Adeno-Associated Virus (AAV) Vectors

A 1965-bp fragment comprising the mouse Tie2 extracellular domain (mTie2-ECD) coding region was obtained from the mTEK plasmid (32), digested with EcoRI and BglII, and inserted into the pVK1 plasmid. The DNA fragment coding for a VSV tag was synthesized, digested with BglII and MluI, and inserted into the mTie2-ECD construct, followed by introduction of the Kozak consensus sequence (33). The mTie2-ECD-VSV fragment was then inserted into a psubCMV-WPRE rAAV expression vector (34). A plasmid coding for mouse Tie2-ECD fused to a FLAG tag was also constructed. The fragment coding for a FLAG sequence was synthesized, digested with BglII and MluI, and inserted into the mTie2-ECD-psubCMV-WPRE plasmid. The recombinant AAVs of serotype 9 were produced as described previously (35), with the exception that the helper plasmid p5E18-VP2/9 was used instead of p5E18-VP2/8 (36). The primer sequences and plasmid constructs are represented in Supplementary Tables 1 and 3 (available online).

Confirmation of AAV Expression by Immunoprecipitation and Immunoblotting

AAV9-sTie2-ECD-FLAG or AAV9-sTie2-ECD-VSV vector, or AAV-HSA as a negative control, was injected into the tibialis anterior muscles of 6- to 8-week-old C57Bl/6 mice (n = 5 in each group, at the dose of 5×10^{11} to 1×10^{12} virus particles [vp] per mouse) anesthetized with the mixture of Ketalar (Pfizer) and Rompun vet (Bayer Healthcare). Expression of the soluble form of Tie2 was confirmed in blood samples taken 2 weeks after the injections. For this, 10-μL samples of serum from each mouse of the same group was pooled and incubated with anti-VSV or anti-FLAG antibodies (Sigma-Aldrich). Proteins were immunoprecipitated with protein G sepharose (Amersham Biosciences), followed by separation by 10% SDS–PAGE, and transferred to a nitrocellulose membrane. The membrane was incubated with anti-Tie2 antibodies (R&D Systems), biotinylated anti-goat secondary antibody (Dako, Glostrup, Denmark; dilution 1:2500 for 30 minutes), followed by streptavidin–biotin horseradish peroxidase conjugate (Amersham Biosciences; dilution 1:8000 for 20 minutes). The

proteins were then detected by enhanced chemiluminescence by using the SuperSignal West Femto Maximum Sensitivity Substrate kit (Thermo Scientific, Rockford, IL).

In Vivo Tumor Assays Using Recombinant AAVs

AAV9-sTie2-ECD or AAV9-HSA was injected intravenously into the lateral tail vein of 6- to 8-week-old female nu/nu BALB/c mice (n = 14 in both groups) at a dose of 5×10^{11} to 1×10^{12} vp per mouse, 3 weeks before implantation of LNM35 cells. The expression of the soluble form of Tie2 was confirmed as described above. LNM35 cells were then implanted subcutaneously into both abdominal flanks of the mice. Once the tumors became readily detectable during the first few days, tumor growth was monitored every second day with measurements using a digital caliper, and the volumes were calculated as described below. For labeling of hypoxic regions within the tumors, pimonidazole (60 mg/kg; Natural Pharmacia International, Burlington, MA) was injected intravenously under anesthesia 1 hour before killing. At the endpoint, the mice were killed and tumors were excised and processed for histology.

Statistical Analysis

Statistical analysis was performed with the unpaired *t* test. Fisher exact test was used for the statistical analysis of metastasis occurrence and repeated measures one-way analysis of variance was used for the analysis of primary tumor growth curves. All statistical tests were two-sided. The values are expressed as means ± 95% confidence interval (CI) in the figures, and as means with the difference of means and 95% confidence intervals in the text. Differences were considered statistically significant at *P* less than .05.

Results

The Effect of Ang2 Overexpression on Metastasis of Human Lung Carcinoma Xenografts

AdAng2 promoted primary LNM35 human lung carcinoma tumor growth when compared with AdLacZ. This increased growth was observed as enhanced bioluminescence of the tumors in AdAng2-transfected mice (AdAng2 [n = 10] vs AdLacZ [n = 9] mice: 25.46×10^5 vs 10.61×10^5 photons/s/cm^2/sr; difference = 14.85×10^5 photons/s/cm^2/sr, 95% CI = 6.51×10^5 to 23.19×10^5 photons/s/cm^2/sr, *P* = .002; Figure 1, A) and as an increase in tumor volume (AdAng2

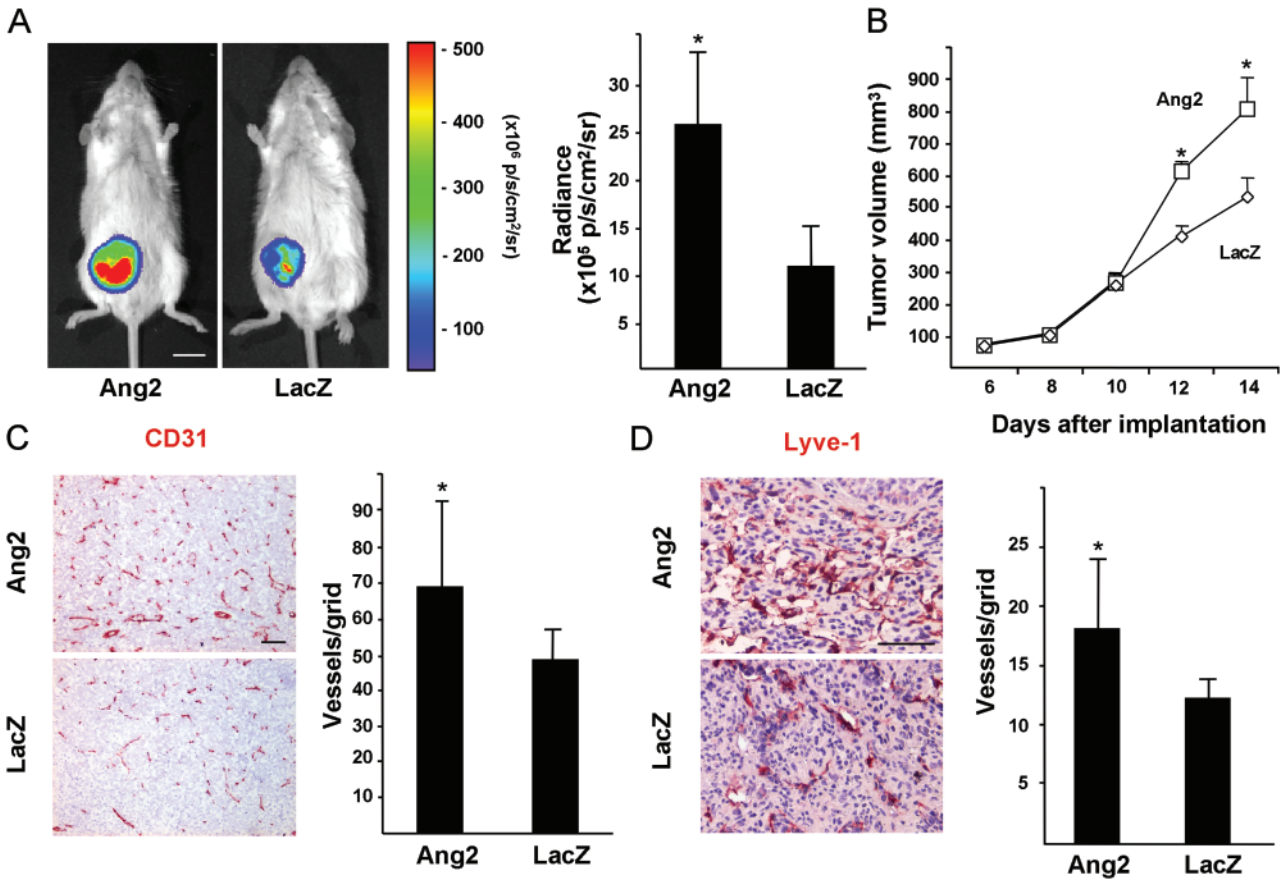

Figure 1. Effect of Ang2 on LNM35 primary tumor growth and vascularization. **A**) Representative images and quantification of bioluminescence of LNM35 tumors in AdAng2- and AdLacZ-treated mice at 14 days after implantation, AdAng2 (n = 10) vs AdLacZ (n = 9) mice. Student's *t* test. **B**) Growth curves of the tumors in (**A**). Repeated measures one-way analysis of variance. **C and D**) Representative immunohistochemical images of CD31- and LYVE-1-stained tumor sections. Samples from at least five mice from both groups were quantified. Quantification of CD31- and LYVE-1-positive vessel densities. Student's *t* test. **Error bars** = 95% confidence intervals. Scale bar in (**A**), 10 mm; in (**C and D**), 200 μm. **P* < .05. All statistical tests were two-sided. Ang2 = Angiopoietin-2; CD31 = cluster of differentiation 31; LacZ = β-galactosidase; LYVE-1 = lymphatic vessel endothelial hyaluronan receptor-1; p/s/cm^2/sr = photons/s/cm^2/steradian.

[n = 10] vs AdLacZ [n = 9] mice: 797 vs 528 mm^3 at day 14; difference = 269 mm^3, 95% CI = 170 to 371 mm^3, n = 9, $P < .001$; Figure 1, B). AdAng2 expression was also associated with an increase in the density of tumor blood vessels (AdAng2 [n = 5] vs AdLacZ [n = 6] mice: 68.43 vs 48.85 vessels per grid; difference = 19.58 vessels per grid, 95% CI = 0.09 to 39.07 vessels per grid, $P = .049$; Figure 1, C) and lymphatic vessels (AdAng2 [n = 5] vs AdLacZ [n = 6] mice: 18.13 vs 12.67 vessels per grid; difference = 5.46 vessels per grid, 95% CI = 1.11 to 9.81 vessels per grid, $P = .019$; Figure 1, D). Importantly, AdAng2 increased regional lymph node metastasis when measured 3 weeks after subcutaneous implantation of LNM35 tumor cells (Figure 2, A and D, and data not shown, a trend for increased bioluminescent signal intensity from lymph nodes in AdAng2 mice ex vivo, AdAng2 vs AdLacZ mice: 6.36×10^7 vs 1.02×10^7

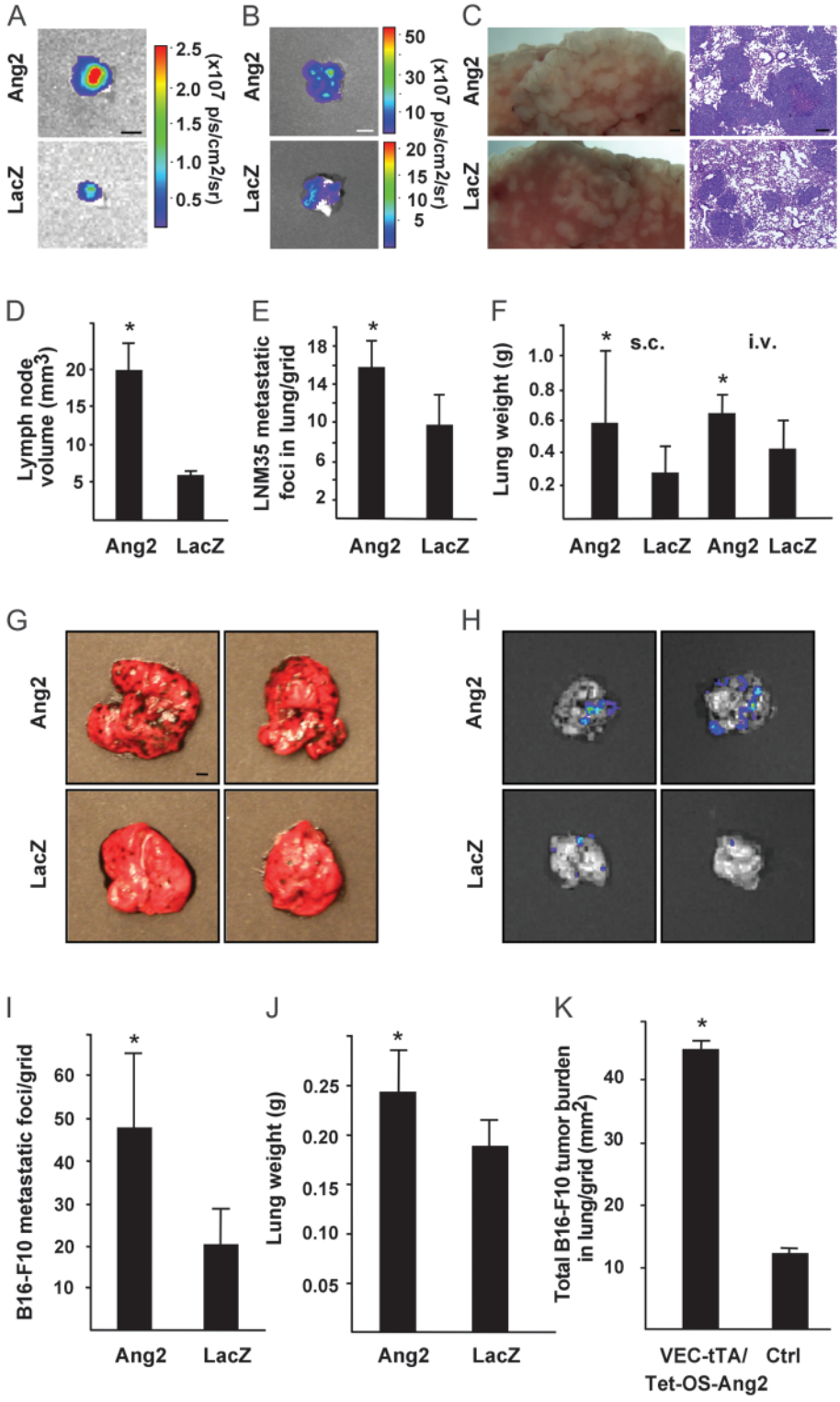

Figure 2. Effect of Ang2 expression on lung metastasis. **A**) Representative bioluminescent images of inguinal lymph nodes 3 weeks after subcutaneous implantation of LNM35 tumors. **B**) Representative ex vivo bioluminescent images of lungs at 7 weeks after implantation of luciferase-positive LNM35 cells into the abdominal subcutis (4 weeks after the excision of the primary tumor). **C**) Representative images of hematoxylin- and eosin-stained lung sections from AdAng2- and AdLacZ-treated mice killed 3 weeks after systemic LNM35 inoculation. **D**) analysis of lymph node volumes, represented in (**A**), AdAng2 (n = 10) vs AdLacZ (n = 9) mice. **E**) Analysis of LNM35 metastatic foci per grid in histological sections from the experiment in (**C**), n = 4 in both groups. **F**) Quantification of lung weights 7 weeks after s.c. tumor cell implantation of LNM35 cells and 3 weeks after i.v. of the tumor cells, AdAng2 (n = 3) vs AdLacZ (n = 6) mice and n = 4 in both groups, respectively. **G**) Representative lungs with B16-F10 metastases in AdAng2- vs AdLacZ-treated mice at 2 weeks after intravenous administration of tumor cells. **H**) Bioluminescent images of lungs with B16-F10 metastatic foci. **I and J**) Analysis of B16-F10 lung metastasis foci per grid (AdAng2 vs AdLacZ) and lung weights, n = 4 in both groups. **K**) Quantification of B16-F10 melanoma tumor burden in conditionally transgenic Ang2 mice (VEC-tTA/Tet-OS-Ang2 mice) and controls, VEC-tTA/Tet-OS-Ang2 mice [n = 5], and control [n = 4] mice. All statistical tests were two-sided Student's *t* tests. **Asterisks** indicate statistically significant differences. **Error bars** = 95% confidence intervals. Scale bar in (**A**) and (**G**), 2 mm; in (**B**), 5 mm; in (**C**), 1 mm (left panel); 100 μm (right panel). Ang2 = Angiopoietin-2; LacZ = β-galactosidase; i.v. = intravenous; s.c. = subcutaneous; p/s/cm^2/sr = photons/s/cm^2/steradian; VEC-tTA/Tet-OS-Ang2 = VE-cadherin-tTA/Tet-OS-Ang2 transgenic mouse.

photons/s/cm²/sr), reflected as a statistically significant increase of inguinal lymph node volume in AdAng2-treated mice (AdAng2 [n = 10] vs AdLacZ [n = 9] mice: 19.82 vs 5.96 mm³; difference = 13.86 mm³, 95% CI = 2.24 to 25.49 mm³, $P = .022$; Figure 2, D).

AdAng2 also promoted metastasis of the LNM35 tumor cells into the lungs, as indicated by a statistically significant increase in lung weight (AdAng2 [n = 3] vs AdLacZ [n = 6] mice: 0.59 vs 0.28 g: difference = 0.31 g, 95% CI = 0.05 to 0.57 g, $P = .027$; Figure 2, F), and a trend for increased bioluminescence signal in the lungs of AdAng2 expressing vs control mice (AdAng2 2.45×10^7 vs AdLacZ 0.33×10^7 photons/s/cm²/sr; Figure 2, B), both measured at 4 weeks after the excision of the primary tumor. Furthermore, Ang2 enhanced the establishment and growth of tumor cell colonies in the lungs at 3 weeks after the intravenous injection of LNM35 cells into immunodeficient NSG mice as evaluated by the lung weight (AdAng2 vs AdLacZ mice: 0.64 vs 0.42 g: difference = 0.21 g, 95% CI = 0.04 to 0.38 g, $P = .02$; Figure 2, F) and the density of metastatic foci in lungs (AdAng2 [n = 4] vs AdLacZ [n = 4] samples: 15.6 vs 9.7 metastatic foci per grid; difference = 6.1, 95% CI = 2.8 to 9.3, $P = .004$; Figure 2, C and E). Similar results were obtained when B16-F10 melanoma cells were used (Figure 2, G–J, metastatic foci per grid in lungs of AdAng2- vs AdLacZ-treated mice [n = 4 in both groups]: 47.1 vs 20.4; difference = 26.6, 95% CI = 11.2 to 42.1, $P = .006$; Figure 2, I).

Expression of Ang2 is induced in the endothelium of hypoxic tumor vessels (15). We analyzed the effect of endothelial Ang2 overexpression on tumor cell metastasis in a conditionally Ang2-overexpressing transgenic mouse model (VEC-tTA/Tet-OS-Ang2), in which the VE-cadherin-tTA construct drives Ang2 expression after the discontinuation of tetracycline administration. Isogenic B16-F10 cells were injected into the tail vein of Ang2-overexpressing mice, and their littermate controls and the lungs were collected 3 weeks after injections. The total lung colony burden was statistically significantly increased in Ang2-overexpressing mice when compared with the controls (VEC-tTA/Tet-OS-Ang2 [n = 5] vs control [n = 4] mice: 45.23 vs 12.26 mm²; difference 32.67 mm², 95 % CI = 31.87 to 34.07, $P < .001$; Figure 2, K).

The Effect of Ang2-Blocking Antibody on Inhibition of Lymphatic and Lung Metastasis

To assess the role of endogenous Ang2 produced by endothelial cells of tumor vessels, we used an Ang2-blocking antibody (27). Luciferase-tagged LNM35 cells were implanted subcutaneously into nu/nu and SCID mice, and after tumor establishment, the mice were randomly assigned to receive 10 mg/kg doses of Ang2-blocking antibody or control hIgG every other day. The Ang2-blocking antibody statistically significantly inhibited primary tumor growth (Figure 3, A and B, tumor weight at excision in nu/nu mice: in Ang2-blocking vs in hIgG group, n = 8 for both groups, 0.84 vs 1.36 g; difference = 0.52 g, 95% CI = 0.81 to 0.23 g, $P = .002$; in SCID mice: in Ang2-blocking group vs in hIgG control mice, n = 10 in both groups, 0.81 vs 1.09 g; difference = 0.28 g, 95 % CI = 0.003 to 0.54 g, $P = .048$) as well as tumor angiogenesis (Ang2-blocking antibody vs hIgG group, n = 8 in both groups, 17.85 vs 21.45 CD31-positive vessels/grid; difference = 3.60, 95% CI = 0.70 to 6.50, $P = .019$; Figure 3, C and D and Supplementary Figure 1, available online), as expected on the basis of previously published data

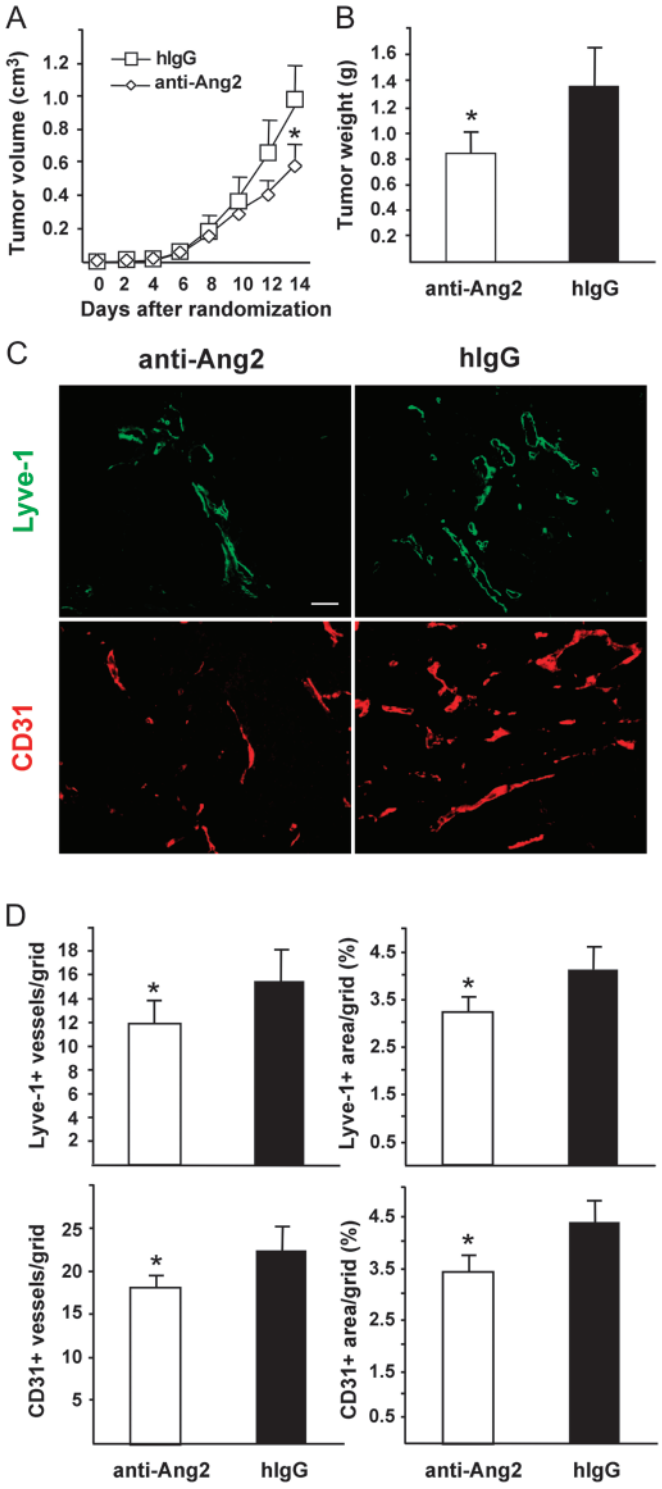

Figure 3. Ang2-blocking antibodies inhibit primary tumor growth, angiogenesis, and lymphangiogenesis. **A**) Growth curves of LNM35 primary tumors in nu/nu mice treated with the Ang2-blocking antibodies or hIgG control, n = 8 in both groups. One-way analysis of variance. **B**) Tumor weights at excision 16 days after implantation, $P = .002$. Student's *t* test. **C**) Representative immunohistochemical images of LYVE-1- and CD31-stained tumor sections. **D**) Quantification of densities and area fractions of Lyve-1-positive lymphatic vessels and of CD31-positive blood vessels from at least five histological sections, $P = .013$ and .019, respectively. Student's *t* test. All statistical tests were two-sided. *$P < .05$. **Error bars** = 95% CI. Anti-Ang2 = angiopoietin-2-blocking antibody; CD31 = cluster of differentiation 31; hIgG = human immunoglobulin G; LYVE-1 = lymphatic vessel endothelial hyaluronan receptor-1. Scale bar, 120 μm.

using Ang2-blocking antibodies in various tumor xenografts (16,19). The Ang2-blocking antibody appeared to induce regression of the endothelium, whereas pericytes and basement membrane structures were detected even after anti-Ang2 antibody treatment (Supplementary Figure 2, available online). Importantly, the Ang2-blocking antibody also attenuated tumor lymphangiogenesis (Ang2-blocking group vs hIgG control group, n = 8 in both groups, 11.95 vs 15.37 LYVE-1-positive vessels per grid; difference = 3.42, 95% CI = 0.85 to 5.98, P = .013; Figure 3, C and D).

Similar to the Ang2-blocking antibodies, administration of the extracellular domain of Tie2 that binds both Ang1 and Ang2 via an AAV vector resulted in an inhibition of LNM35 tumor growth and angiogenesis (Supplementary Figure 3, available online), consistently with the previously reported results (37).

To analyze the effect of Ang2-blocking antibodies on tumor metastasis, we measured tumor cell dissemination into the regional (inguinal) lymph nodes. The rate of lymph node metastasis and lymph node weight at the time of excision of primary tumors were decreased in SCID mice treated with the Ang2-blocking antibodies (10% in the anti–Ang2-treated group vs 70% in control hIgG group) (Figure 4, A–C, lymph node weight: P = .020 [SCID, lower panel, Figure 4, C] to P = .043 [nu/nu, upper panel, Figure 4, C]). There was a clear trend of inhibition of the metastatic dissemination of tumor cells into axillary lymph nodes of SCID mice as evaluated by the occurrence of metastasis (data not shown, 0/10 in Ang2-blocking group vs 4/10 in hIgG group) and the occurrence of cytokeratin-positive cells (Figure 4, D).

To evaluate whether Ang2 blockade affected homing of tumor cells into the lungs, luciferase-tagged LNM35 cells were injected intravenously into mice receiving the Ang-blocking antibody or hIgG and analyzed by the bioluminescent signal intensity from the excised lungs at 5 days. The anti-Ang2 antibody treatment decreased the metastatic burden in the lungs (Ang2-blocking antibody vs hIgG: 103.4 vs 225.6 photons/s/cm^2/sr, n = 3 in both groups, two independent studies, difference = 122.2, 95% CI = 38.4 to 206.0, P = .016; Figure 5, A and B). The metastatic foci in the lungs were also analyzed at 8 days after systemic inoculation of GFP-tagged tumor cells. The Ang2-blocking antibody inhibited lung metastasis formation statistically significantly (Ang2-blocking antibody [n = 4] vs hIgG [n = 3], 12.2 vs 22.4 LNM35 cell clusters per grid; difference = 10.2, 95% CI = 5.6 to 14.9, P = .002; Figure 5, C and E). The inhibition of LNM35 lung metastasis by the Ang2-blocking antibody was also evident at the later time point of 2 weeks (tumor area per grid in Ang2-blocking antibody vs hIgG groups, n = 4 in both groups: 14.78% vs 24.33%; difference = 9.55, 95% CI = 3.12 to 15.98, P = .011; Figure 5, H left; and lung weight: Ang2-blocking antibody vs hIgG 0.22 vs 0.27 g, difference = 0.05 g, 95% CI = 0.01 to 0.09 g, P = .017, Figure 5, H right). In contrast, overexpression of Ang2 promoted tumor metastasis into the lungs when analyzed 4 days after inoculation of the GFP-tagged LNM35 or LLC tumor cells (LLC cell cluster density in AdAng2 vs AdLacZ group, n = 4 in both groups, 35.7 vs 28.9, difference = 6.8, 95% CI = 1.7 to 12.0, P = .018; LNM35 cell cluster density in AdAng2 vs AdLacZ group, n = 4 in both groups, 6.17

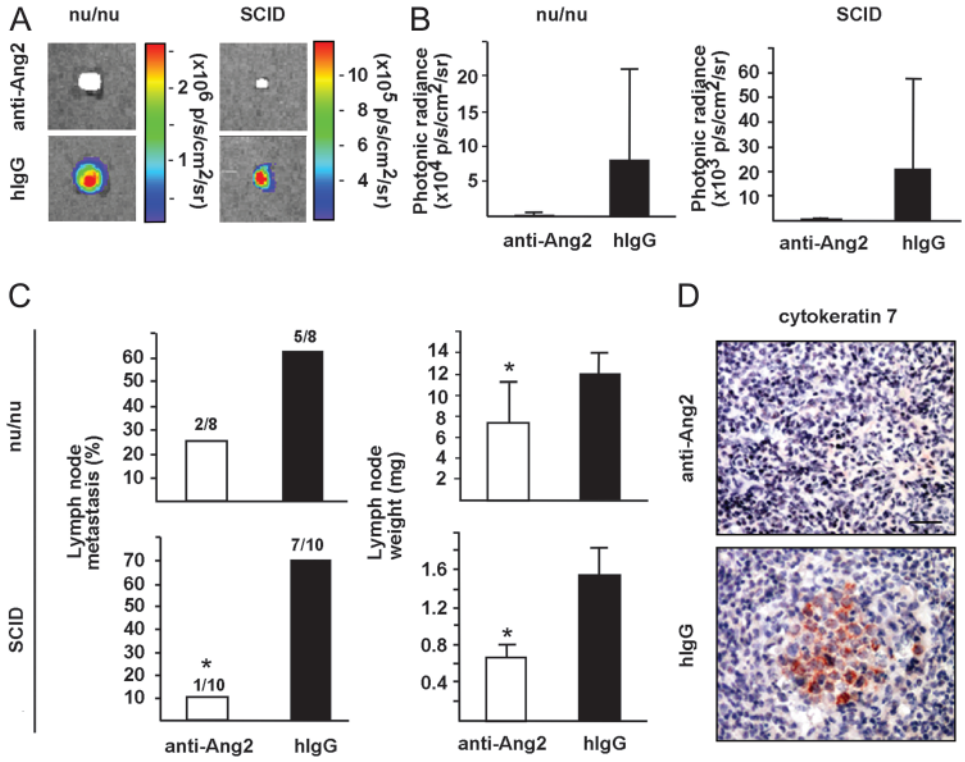

Figure 4. Ang2-blocking antibodies inhibit lymphatic metastasis. **A**) Representative ex vivo bioluminescent images of the regional inguinal lymph nodes in nu/nu and SCID mice, excised at 16 days after subcutaneous tumor implantation, n = 8 and n = 10 in both groups, respectively. **B**) Quantification of bioluminescence emission from the regional lymph nodes. **C**) Occurrence of metastasis in regional lymph nodes, and lymph node weights, P = .020 to P = .043. **D**) Representative images of intranodal cytokeratin 7–positive immunostaining in axillary lymph nodes excised from Ang2-blocking antibody and hIgG-treated nu/nu mice. **Error bars** = 95% confidence intervals. *P < .05. Anti-Ang2 = angiopoietin-2-blocking antibody; hIgG = human immunoglobulin G; p/s/cm^2/sr = photons/s/cm^2/steradian. Student's t test. All statistical tests were two-sided. Scale bar in (**A**), 2 mm, in (**D**), 40 μm.

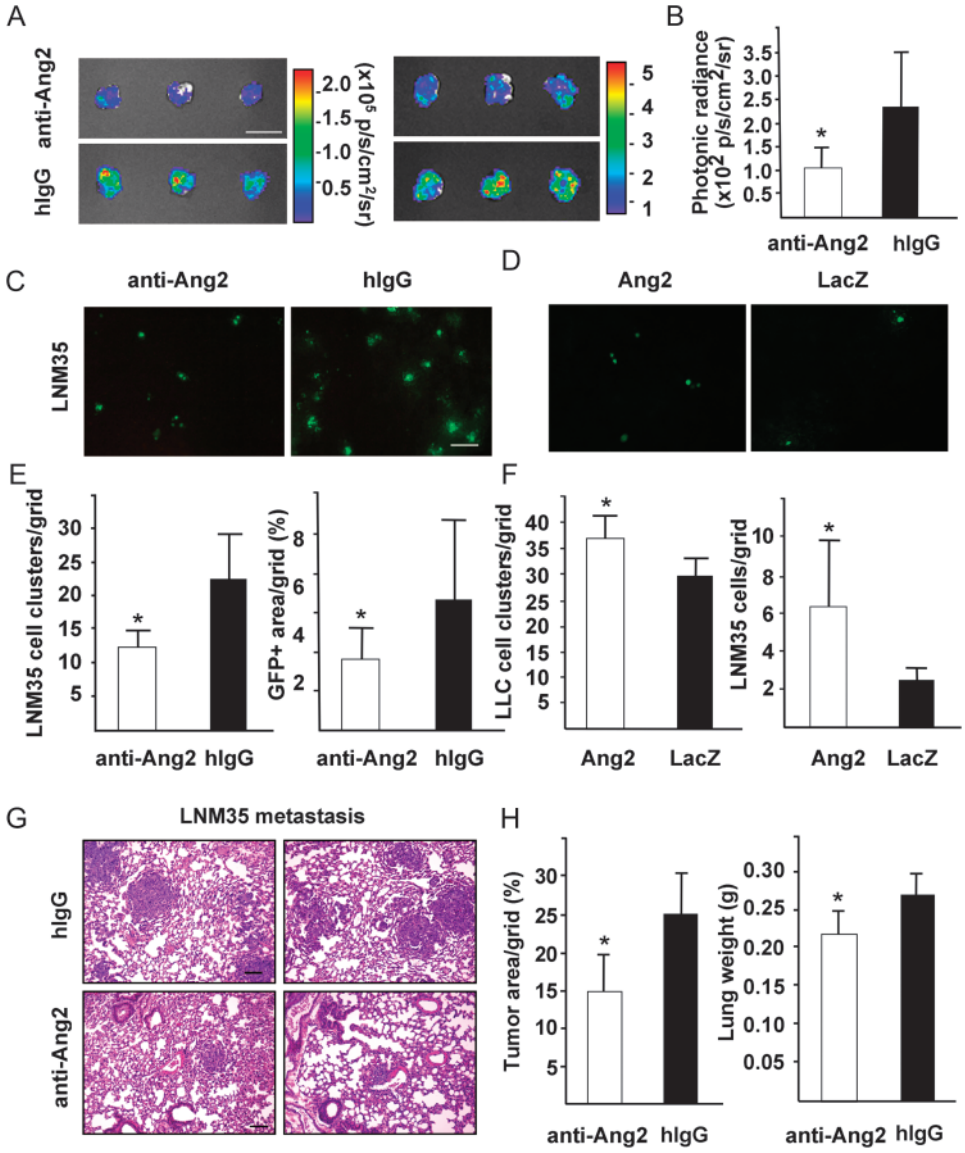

Figure 5. Ang2 overexpression induces and Ang2-blocking antibodies suppress formation of metastatic foci in lungs. **A**) Bioluminescent images of lungs from Ang2-blocking antibody and hIgG control–treated NSG mice 5 days after systemic inoculation of luciferase-positive LNM35 cells. Two independent studies with similar results. **B**) Quantification of bioluminescent signal intensities, n = 3 in both groups, $P = .016$. **C** and **D**) Representative fluorescent micrographs of lung sections with foci of GFP-positive LNM35 metastatic cells at 8 days after intravenous inoculation of the cells into Ang2-blocking antibody vs hIgG-treated mice (**C**), and at 4 days after systemic inoculation into the tail vein of mice treated with AdAng2 or AdLacZ (**D**). **E**) Analysis of GFP-positive LNM35 foci and GFP signal area fraction in lung tissues of mice treated with Ang2-blocking antibodies or hIgG control, n = 4 in anti-Ang2 antibody group, n =3 in hIgG group. **F**) Quantification of the homing of intravenously injected GFP-positive LLC and LNM35 tumor cells into the lungs of AdAng2- or AdLacZ-treated mice, n = 4 in both groups, $P = .019$. **G**) Representative HE-stained lung sections with LNM35 metastatic foci analyzed 2 weeks after intravenous inoculation of the tumor cells to mice treated with Ang2-blocking antibodies vs hIgG. **H**) Quantification of metastatic area fraction in HE-stained sections and lung weights at excision, $P = .028$. **Error bars** = 95% confidence intervals. Scale bar in (**A**), 15 mm. Anti-Ang2 = angiopoietin-2-blocking antibody; GFP = green fluorescent protein; hIgG = human immunoglobulin G; NSG = NOD SCID gamma; p = photons; p/s/cm²/sr = photons/s/cm²/steradian. *$P < .05$. Student's *t* test. All statistical tests were two-sided.

vs 2.67, difference = 3.50, 95% CI = 0.81 to 6.19, $P = .019$; Figure 5, D and F).

Effects of Endothelial Ang2 Overexpression and Ang2-Blocking Antibody on Vascular Integrity in Lung Metastases

To explain the effects of Ang2 overexpression and Ang2-blocking antibody on lung metastasis, we investigated their effects on the ultrastructure of the endothelial barrier. Endothelial cell–cell junctions and cell adhesion to the underlying basement membrane were analyzed by transmission electron microscopy in metastasis-associated blood capillaries in the lung colonization assay in conditional Ang2-overexpressing, Ang2-blocking antibody-treated and control mice. The metastasis-associated capillaries in the Ang2-overexpressing mice showed more frequent and profound alterations in capillary morphology compared with wild-type mice

(percent of analyzed capillaries, Ang2-overexpressing [n = 132] vs control mice [n = 130]: 66.5% vs 20.2%). These abnormalities included endothelial cell detachment from the basement membrane (Ang2-overexpressing vs control mice: 49.6% vs 12.2%) and less extensive endothelial cell–cell junctions or even gaps between the endothelial cells (24.3% vs 8.1%) (Figure 6, A–D). The Ang2-blocking antibodies reduced endothelial cell swelling and heterogeneity of metastasis-associated capillaries in the NSG mice and showed more prominent endothelial adherens junctions when compared with capillaries adjacent to the metastases in HSA control mice (Figure 6, E–H and Supplementary Figure 4, available online).

Influence of Ang2-Blocking Antibody on Postnatal Retinal Angiogenesis

Neonatal retinal angiogenesis is dependent on Ang2 expression (12), and blocking Ang2 has been found to inhibit retinal angiogenesis (27). To further investigate the role of Ang2 during physiological retinal angiogenesis, we injected Ang2-blocking or control antibodies to newborn NMRI pups during postnatal days P0–P4. In line with results from a parallel independent study (27), we observed a statistically significant decrease in retinal vascularization in the Ang2-blocking antibody-treated pups when compared with the control group. In addition, we found decreased branching density (Supplementary Figure 5, A and B, available online) and vascular tuft-like structures located at the edge of the advancing vessel network (Supplementary Figure 5, A, available online) in the Ang2-blocking antibody-treated pups Tie2 was expressed in the retinal vessels, except for the tip cells. However, reduced Tie2 staining was detected in the angiogenic front of anti-Ang2 antibody treated pups, whereas the expression of the receptor in the rest of the retina was not altered (Supplementary Figure 5, C, available online). High-resolution imaging of the retinas treated with Ang2-blocking antibody revealed isolated patterns of pericytes that were not associated with endothelial cells (Supplementary Figure 5, D and E, available online), suggestive of vessel regression or failed sprouts.

The Effect of Blocking Ang2 Antibodies on Ligand-Induced Cellular Trafficking of the Tie2 Receptor

To study the cellular mechanisms responsible for the in vivo effects of the Ang2-blocking antibody, we analyzed its effects on cultured microvascular endothelial cells. Our previous results (30) and those of Fukuhara et al. (38) have recently shown that Ang1 induces a distinct Tie2 signaling complex at endothelial cell–cell contacts, where it provides survival and stability signals and induces phosphorylation of the endothelial nitric oxide synthetase (eNOS) (30,38). In the previous report, Ang2 was found to compete with Ang1 for receptor binding at the cell–cell junctions (30). To elucidate the effects of the Ang2-blocking antibodies on this process, endothelial cells expressing Tie2 fluorescently tagged with GFP were treated with the Ang2-blocking or control antibodies. In microvascular lymphatic and blood vascular endothelial cells, which produce Ang2 in culture (39), Tie2 and Ang2 were localized at the cell–cell junctions (Figure 7, A and B). However, autocrine Ang2 induced only weak Tie2 phosphorylation and almost no eNOS phosphorylation when compared with exogenously provided Ang1 (Figure 7, A, Supplementary Figure 6, A, available online).

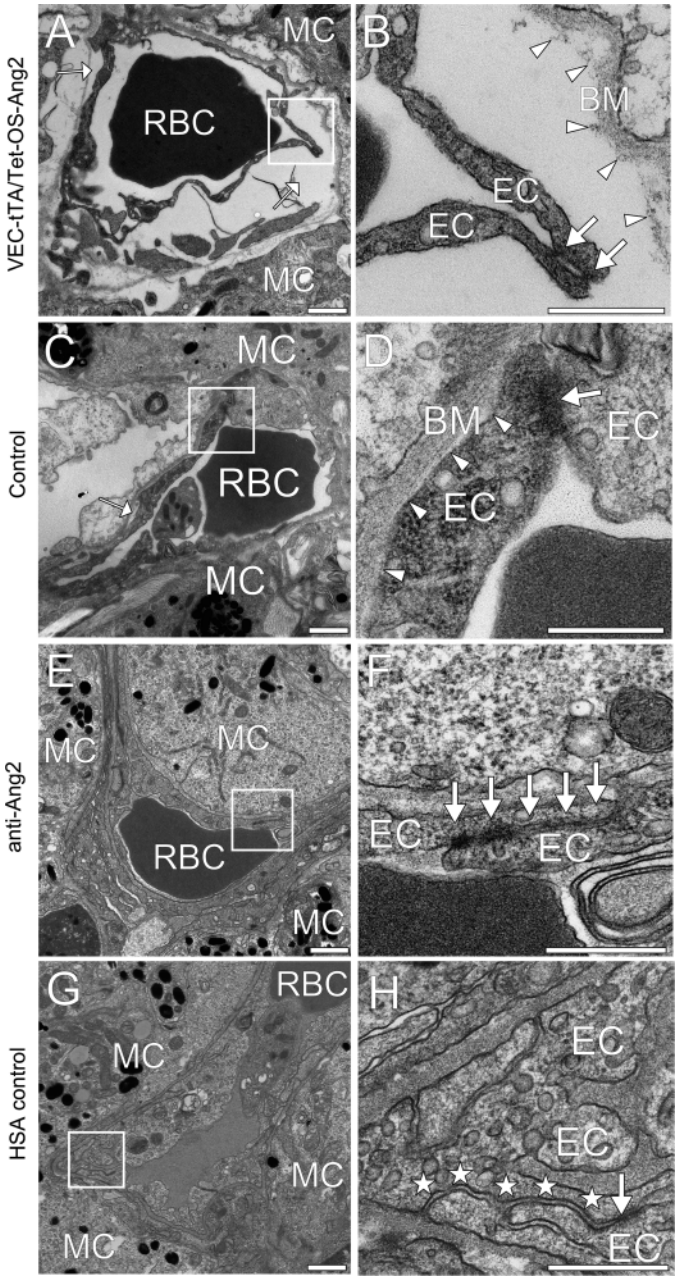

Figure 6. Effect of Ang2-blocking antibodies on endothelial cell–cell junctions in lung metastases and Ang2 overexpression on vascular integrity. Transmission electron micrographs (TEM) of capillaries adjacent to metastatic B16-F10 melanoma cell (MC) colonies of Ang2-overexpressing (**A** and **B**) and control C57Bl/6J mice (**C** and **D**). TEM micrographs of Ang2-blocking antibody (**E** and **F**) and HSA-treated (**G** and **H**) metastases of NSG mice, samples from at least three mice were evaluated. (**B**), (**D**), (**F**), and (**H**) show the **boxed areas** at a higher magnification. Note that in the Ang2-overexpressing mice, the capillaries show more structural abnormalities in endothelial cell (EC), basement membrane (BM) adhesions and less extensive endothelial cell–cell junctions (**arrows** in **B** and **D**) than in the control mice. **Arrowheads** in (**B**) and (**D**) indicate the interface between the ECs and the BM. Note also that the Ang2-blocking antibody treatment has a normalizing effect; the endothelium in the HSA-treated lung metastasis has less prominent (**stars**) junctional complexes (**arrows**) and uneven EC layering. Scale bar in (**A**), (**C**), (**E**), and (**G**), 1 μm; in (**B**), (**D**), (**F**), and (**H**), 500 nm. Anti-Ang2 = angiopoietin-2-blocking antibody; HSA = human serum albumin; NSG = NOD SCID gamma; RBC = red blood cell; VEC-tTA/Tet-OS-Ang2 = VE-cadherin-tTA/Tet-OS-Ang2 transgenic mouse.

The Ang2-blocking antibody induced internalization of Ang2, leading to decreased Tie2 and Tie1 receptor localization and Tie2 phosphorylation at the endothelial cell–cell contacts (Figures 7, A and B and 8 and Supplementary Figure 7, available online). In contrast, the Ang2-blocking antibody did not inhibit Ang1-stimulated Tie2 localization and phosphorylation at cell–cell contacts, indicating specific blockade of only the Ang2 signals (Figure 7, A). Internalized vesicles containing Ang2 were observed at 30 minutes of treatment with Ang2-blocking antibodies, but after 5 hours, they were no longer visible (Figure 8). Decreased formation of

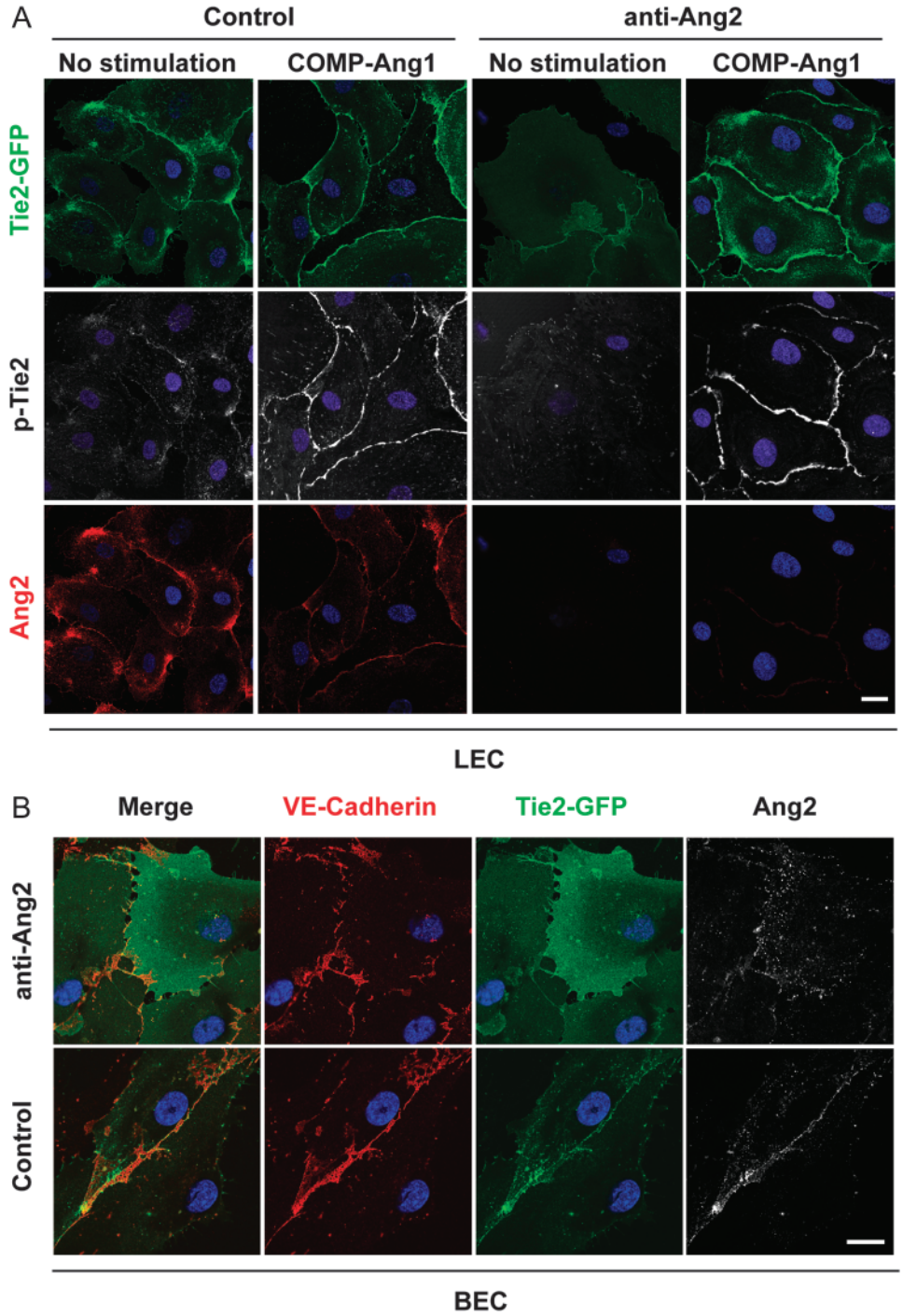

Figure 7. Ang2-blocking antibody inhibits the formation of Ang2-induced Tie2 signaling complexes. **A**) Human dermal microvascular lymphatic endothelial cells (LECs) were transfected with the Tie2-GFP retrovirus. The cells were treated with Ang2-blocking antibody (48 hours) or left untreated, followed by stimulation with COMP-Ang1 (30 minutes). The cells were fixed, permeabilized, and stained for Ang2 and phosphorylated Tie2 (P-Tie2). Note that the Ang2-blocking antibody inhibits Tie2 translocation induced by endogenous Ang2 but not by exogenous COMP-Ang1 added to the cultures. **B**) Blood vascular endothelial cells (BECs) were transfected with Tie2-GFP and treated for 30 minutes with Ang2-blocking antibody or hIgG as a control. The cells were fixed, permeabilized, and stained for VE-cadherin or Ang2. The Ang2-blocking antibody inhibits Ang2-induced Tie2 translocation also in the BECs. Nuclear DAPI stain. Confocal images. Scale bar, 20 μm. Anti-Ang2 = angiopoietin-2-blocking antibody; COMP-Ang1 = cartilage oligomeric matrix protein–angiopoietin-1; hIgG = human immunoglobulin G.

Ang2-Tie2 complexes was also detected following transfection of Tie2-GFP expressing cells with siRNA oligonucleotides to silence Ang2 expression (Supplementary Figure 6, B, available online).

We further analyzed the internalization of cell surface–bound anti-Ang2 antibody in LECs. To this end, the anti-Ang2 antibodies were incubated with cells on ice and either directly subjected to glycine wash for depletion of the cell surface or incubated at 37°C to allow internalization of cell surface bound antibodies. The acid wash completely removed cell surface–bound antibodies (0% remained from maximal binding), but the internalized antibodies were retained in the cells (11% remained from maximal binding, Supplementary Figure 8, available online). These data indicate that the anti-Ang2 antibody is partially internalized into LECs in vitro.

To investigate the effect of tumor cells on Ang2-induced Tie2 signaling, we cultured Tie2-GFP expressing blood vascular endothelial cells on Transwell filters in the presence or absence of the LNM35 lung carcinoma cells in the lower compartment. Notably, Ang2-Tie2 complexes were increased in the endothelial cell junctions in the presence of the LNM35 tumor cells, whereas complex formation was blocked by the Ang2-blocking antibodies (Supplementary Figure 9, available online). These results suggest that the Ang2-blocking antibodies are associated with decreased expression of Ang2-Tie2 complexes while leaving Ang1-Tie2 complexes intact at endothelial cell–cell junctions.

Discussion

Our results indicate that Ang2 increases tumor metastasis at least in part by promoting endothelial disruption and increasing tumor cell translocation and homing to target organs. We also provide mechanistic insight into the effects of the antibody-mediated blockade of Ang2 at the cellular level. To address the function of Ang2 in tumor metastasis, we used systemic and endothelial cell-specific Ang2 overexpression, as well as Ang2-blocking antibodies in various tumor models. Our results demonstrate that systemic Ang2 overexpression promotes tumor lymphangiogenesis as well as lymph node and lung metastasis in addition to tumor growth and angiogenesis. Ang2 also enhanced the establishment of metastatic colonies in the lungs after intravenous tumor cell inoculation. Importantly, by using VEC-tTA/Tet-OS-Ang2 transgenic mice, in which Ang2 is specifically induced only in the vascular endothelium, we demonstrated that endothelial overexpression of Ang2 increases lung metastasis. Alternatively, Ang2 blockade attenuated tumor lymphangiogenesis, dissemination of tumor cells via the lymphatic vessels, lung metastasis, and tumor cell colonization of the lungs.

The antiangiogenic effects of specific Ang2 blockade on tumor growth and vascularization have been previously characterized using Ang2 blocking in various tumor xenografts, but the effects on tumor metastasis were not investigated (16,18,19,27). In one report, intrapleural injection of lentiviral Ang2 short hairpin

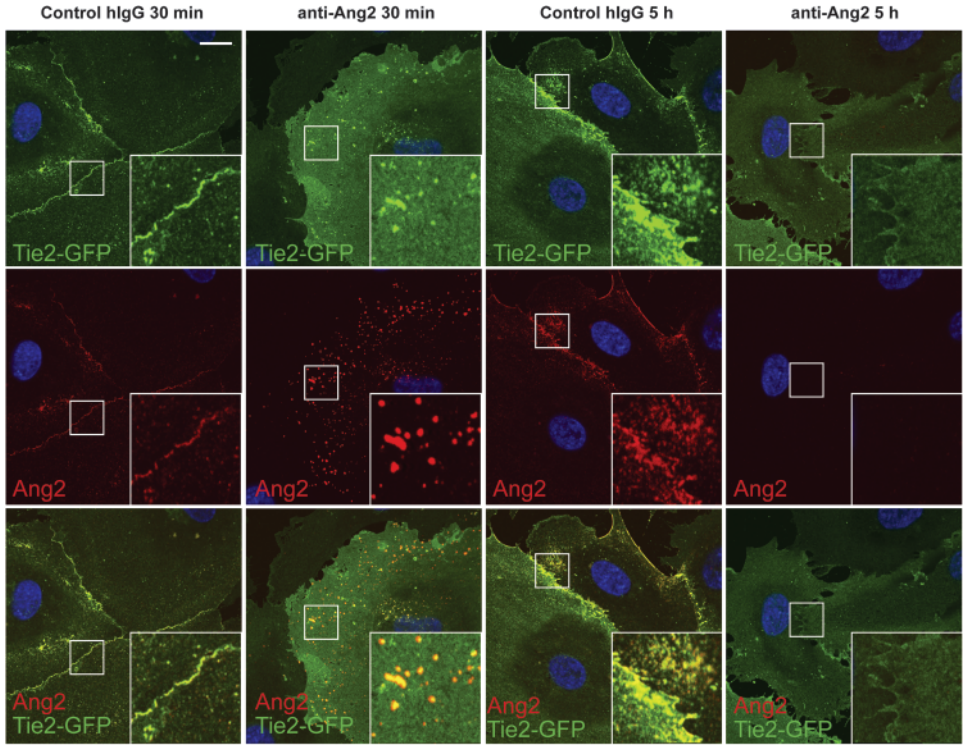

Figure 8. Ang2-blocking antibody induces internalization of the Ang2-Tie2 complexes. BECs transfected with Tie2-GFP retrovirus were treated with Ang2-blocking or hIgG control antibody for the indicated periods. The cells were fixed, permeabilized, and stained for Ang2. Note that the Ang2-blocking antibody, but not control antibody, induces transient internalization of Ang2 and Tie2 in intracellular vesicles, evident at 30 minutes, whereas no vesicles are present at 5 hours after Ang2-blocking antibody treatment. Nuclear DAPI stain. Confocal images. Scale bar, 20 μm. Ang2 = Angiopoietin-2-detecting antibody; Anti-Ang2 = angiopoietin-2-blocking antibody; BEC = blood microvascular endothelial cells; hIgG = human immunoglobulin G.

RNA in mice bearing mammary tumor xenografts was reported to inhibition endothelial permeability in the lungs (40). In another report, Ang2 overexpression in tumor cells increased their invasive properties by an autocrine, Tie2-independent effect mediated via the integrins (9). However, only a minor fraction of human tumor cell lines express detectable amounts of Ang2 (1). Importantly, the lung cancer cells we used expressed no detectable Ang2 in culture, unlike in previous studies in which Ang2 inhibitors were used (16,41).

Targeted deletion of Ang2 leads to defective blood vessel development in the eye and lymphatic vessel development in the mesenterium and skin (12). In the developing postnatal retina, the Ang2-blocking antibody was found to delay vascularization (27), which was confirmed in our study. Further analysis showed that blocking Ang2 induced vascular tuft-like structures at the angiogenic front, where signs of sporadic sprout regression were observed. In the primary tumors treated with the Ang2-blocking antibody, basement membrane and pericyte marker–positive and endothelial cell negative vessel structures were present, similarly indicating endothelial regression. These results are consistent with the data that autocrine Ang2 contributes to endothelial cell survival and migration in some contexts (10,42, our unpublished results using Ang2-blocking antibody). In mice surviving Ang2 deletion, an initial delay was observed in the growth of isogenic tumors (17); however, in our study, the Ang2-blocking antibodies also induced statistically significant inhibition in the later phases of tumor growth. Thus, it is possible that genetic deletion of Ang2 and blocking antibodies against Ang2 have different mechanisms of action.

We (30) and Fukuhara et al. (38) have previously shown that angiopoietins induce the formation of unique Tie2 receptor complexes in endothelial cells (30,38). In cells with established contacts to other cells, Ang1 and Ang2 were found to trigger Tie2 translocation to cell–cell junctions, where Ang1 has been shown to reduce paracellular permeability (30,38,43). Here, we show that autocrine Ang2 secreted by endothelial cells similarly induces Tie2 and Tie1 translocation to cell–cell contacts. However, in contrast to Ang1, Ang2 induced only weak Tie2 phosphorylation and may thus decrease Ang1 signals via the Tie receptors in the endothelial cell–cell junctions (30). When the endothelial cells were cocultured with the tumor cells, the presence of Ang2-Tie2 complexes was increased in the endothelial cell–cell junctions, even when the cells were under normal oxygen pressure. The Ang2-blocking antibody inhibited endothelial Ang2 function by inducing the internalization of the Ang2-Tie2 receptor complexes and by inhibiting the subsequent formation of such complexes. Because of the multimeric nature of Ang2, the anti-Ang2 antibody may result in the formation of large receptor clusters on the cell surface; these could be more effectively targeted for endocytosis. The Ang1-induced Tie receptor complexes were not affected by the Ang2 antibody. Because only the Ang2-bound Tie2 receptor fraction was directed for internalization, the results suggest that during Ang2 blocking in the metastatic lungs, Ang1 can bind and activate Tie2, contributing to stabilization of endothelial cell–cell junctions.

Our results showed that fewer tumor cell colonies were established in the lungs of mice treated with the Ang2-blocking antibody when compared with control antibody–treated mice at the relatively early time points when angiogenesis was not yet detected in the metastatic foci. Although we have not imaged extravasation per se, these results suggest that blocking Ang2 inhibited the extravasation of tumor cells to the lungs or the very early stages of metastatic colony establishment. It was previously shown that the tumor cell–associated lung capillaries express increased amounts of Ang2 (15). In the pulmonary vessels associated with the lung metastases, the Ang2-blocking antibody seemed to counteract the disruption of the endothelial cell–cell junctions and vascular integrity, suggesting that by decreasing cell–cell adhesion and endothelial integrity, endogenous Ang2 can facilitate the extravasation step at the endothelial cell–cell junctions. How Ang2 leads to the disruption of endothelial integrity remains to be elucidated. Such a mechanism may involve binding to integrins and loss of EC-EC junctional complexes, as reported for the related angiopoietin-like 4 (Angptl4) protein (44).

Although we show that the Ang2-blocking antibodies inhibit metastasis in immunodeficient mice in the absence of inflammatory cell contribution, Ang2 also affects the inflammatory and immune responses in tumors (45,46). Ang2 has been reported to stimulate Tie2-expressing monocytes to suppress T-cell activation and to promote regulatory T-cell expansion (45). In tumor-bearing immunocompetent mice, Ang2-blocking antibodies interfered with Tie2 expression in a subpopulation of macrophages and decreased angiogenesis, resulting in inhibition of metastasis (46). We found that the disruption of endothelial cell–cell and cell–matrix contacts in metastatic pulmonary capillaries was further aggravated in an immunocompetent background, suggesting that the immune response can contribute to endothelial destabilization.

This study had some limitations. We used rapidly growing tumors. Thus, the conclusions may be strengthened with the use of genetically engineered mouse tumor models. The dose–response range was not evaluated, and because of the rapid tumor growth and treatment schedules, possible adverse effects related to the treatment may have gone unnoticed. In addition, it remains to be investigated if the Ang2 antibodies can inhibit metastatic colonization of other tissues besides the lungs.

Our results are in line with the previously proposed model in which Ang2 becomes initially overexpressed in the tumor co-opted blood vessels, leading to vessel destabilization. This increases hypoxia in the tumor, and the expression of hypoxia-regulated VEGF and Ang2 growth factors, inducing robust tumor angiogenesis (47). The results from a study in which Ang2 was ectopically expressed in a mammary carcinoma cell line also support a model of dual action of Ang2 in the tumors (48). In that study, Ang2 expression induced intratumoral hemorrhage, non-functional and abnormal blood vessels, and was associated with pericyte loss and increased endothelial cell apoptosis, possibly because of imbalance of the Ang2 and VEGF levels in the tumors (48). It has been claimed that VEGFR2-targeted anti-angiogenic therapy increases metastatic frequency in some preclinical animal models (49). Our results showing that Ang2 induces vascular destabilization during tumor metastasis suggest that during VEGF blockade, Ang2-induced vascular destabilization could be associated with increased metastasis. Thus, combinatory therapy blocking both VEGF and Ang2 may provide more effective tumor growth and metastasis inhibition.

In conclusion, we show that Ang2 contributes substantially to tumor progression and that blocking of Ang2 inhibits endothelial destabilization and constitutes an efficient strategy for inhibition of tumor growth and metastatic dissemination. Our data thus provide important new insights into the Ang2/Tie2 signaling pathway as an attractive target for cancer therapy.

References

1. Augustin HG, Koh GY, Thurston G, Alitalo K. Control of vascular morphogenesis and homeostasis through the angiopoietin-Tie system. *Nat Rev Mol Cell Biol.* 2009;10(3):165–177.
2. Holopainen T, Huang H, Chen C, et al. Angiopoietin-1 overexpression modulates vascular endothelium to facilitate tumor cell dissemination and metastasis establishment. *Cancer Res.* 2009;69(11):4656–4664.
3. Davis S, Aldrich TH, Jones PF, et al. Isolation of angiopoietin-1, a ligand for the TIE2 receptor, by secretion-trap expression cloning. *Cell.* 1996; 87(7):1161–1169.
4. Dumont DJ, Gradwohl G, Fong GH, et al. Dominant-negative and targeted null mutations in the endothelial receptor tyrosine kinase, tek, reveal a critical role in vasculogenesis of the embryo. *Genes Dev.* 1994;8(16):1897–1909.
5. Suri C, Jones PF, Patan S, et al. Requisite role of angiopoietin-1, a ligand for the TIE2 receptor, during embryonic angiogenesis. *Cell.* 1996;87(7): 1171–1180.
6. Sato TN, Tozawa Y, Deutsch U, et al. Distinct roles of the receptor tyrosine kinases Tie-1 and Tie-2 in blood vessel formation. *Nature.* 1995;376(6535): 70–74.
7. Kim I, Kim HG, So JN, Kim JH, Kwak HJ, Koh GY. Angiopoietin-1 regulates endothelial cell survival through the phosphatidylinositol 3'-Kinase/Akt signal transduction pathway. *Circ Res.* 2000;86(1):24–29.
8. Maisonpierre PC, Suri C, Jones PF, et al. Angiopoietin-2, a natural antagonist for Tie2 that disrupts in vivo angiogenesis. *Science.* 1997;277(5322): 55–60.
9. Imanishi Y, Hu B, Jarzynka MJ, Guo P, Elishaev E, Bar-Joseph I, et al. Angiopoietin-2 stimulates breast cancer metastasis through the alpha(5) beta(1) integrin-mediated pathway. *Cancer Res.* 2007;67(9):4254–4263.
10. Yuan HT, Khankin EV, Karumanchi SA, Parikh SM. Angiopoietin 2 is a partial agonist/antagonist of Tie2 signaling in the endothelium. *Mol Cell Biol.* 2009;29(8):2011–2022.
11. Lobov IB, Brooks PC, Lang RA. Angiopoietin-2 displays VEGF-dependent modulation of capillary structure and endothelial cell survival in vivo. *Proc Natl Acad Sci U S A.* 2002;99(17):11205–11210.
12. Gale NW, Thurston G, Hackett SF, et al. Angiopoietin-2 is required for postnatal angiogenesis and lymphatic patterning, and only the latter role is rescued by Angiopoietin-1. *Dev Cell.* 2002;3(3):411–423.
13. Fagiani E, Lorentz P, Kopfstein L, Christofori G. Angiopoietin-1 and -2 exert antagonistic functions in tumor angiogenesis, yet both induce lymphangiogenesis. *Cancer Res.* 2011;71(17):5717–5727.
14. Stratmann A, Risau W, Plate KH. Cell type-specific expression of angiopoietin-1 and angiopoietin-2 suggests a role in glioblastoma angiogenesis. *Am J Pathol.* 1998;153(5):1459–1466.
15. Holash J, Wiegand SJ, Yancopoulos GD. New model of tumor angiogenesis: dynamic balance between vessel regression and growth mediated by angiopoietins and VEGF. *Oncogene.* 1999;18(38):5356–5362.
16. Falcón BL, Hashizume H, Koumoutsakos P, et al. Contrasting actions of selective inhibitors of angiopoietin-1 and angiopoietin-2 on the normalization of tumor blood vessels. *Am J Pathol.* 2009;175(5):2159–2170.
17. Nasarre P, Thomas M, Kruse K, et al. Host-derived angiopoietin-2 affects early stages of tumor development and vessel maturation but is dispensable for later stages of tumor growth. *Cancer Res.* 2009;69(4):1324–1333.
18. Oliner J, Min H, Leal J, et al. Suppression of angiogenesis and tumor growth by selective inhibition of angiopoietin-2. *Cancer Cell.* 2004;6(5): 507–516.
19. Brown JL, Cao ZA, Pinzon-Ortiz M, et al. A human monoclonal anti-ANG2 antibody leads to broad antitumor activity in combination with VEGF inhibitors and chemotherapy agents in preclinical models. *Mol Cancer Ther.* 2010;9(1):145–156.
20. Schulz P, Fischer C, Detjen KM, et al. Angiopoietin-2 drives lymphatic metastasis of pancreatic cancer. *FASEB J.* 2011;25(10):3325–3335.
21. Sarao R, Dumont DJ. Conditional transgene expression in endothelial cells. *Transgenic Res.* 1998;7(6):421–427.
22. Lohela M, Heloterä H, Haiko P, Dumont DJ, Alitalo K. Transgenic induction of vascular endothelial growth factor-C is strongly angiogenic in mouse embryos but leads to persistent lymphatic hyperplasia in adult tissues. *Am J Pathol.* 2008;173(6):1891–1901.
23. Sun JF, Phung T, Shiojima I, et al. Microvascular patterning is controlled by fine-tuning the Akt signal. *Proc Natl Acad Sci U S A.* 2005;102(1): 128–133.
24. Kozaki K, Miyaishi O, Tsukamoto T, et al. Establishment and characterization of a human lung cancer cell line NCI-H460-LNM35 with consistent lymphogenous metastasis via both subcutaneous and orthotopic propagation. *Cancer Res.* 2000;60(9):2535–2540.
25. Karpanen T, Heckman CA, Keskitalo S, et al. Functional interaction of VEGF-C and VEGF-D with neuropilin receptors. *FASEB J.* 2006;20(9): 1462–1472.
26. Cho CH, Kammerer RA, Lee HJ, et al. COMP-Ang1: a designed angiopoietin-1 variant with nonleaky angiogenic activity. *Proc Natl Acad Sci U S A.* 2004;101(15):5547–5552.
27. Leow CC, Koffman K, Inigo I, et al. MEDI3617, a human anti-Angiopoietin 2 monoclonal antibody, inhibits angiogenesis and tumor growth in human tumor xenograft models. *Int J Oncol.* In press.
28. Kim KE, Cho CH, Kim HZ, Baluk P, McDonald DM, Koh GY. In vivo actions of angiopoietins on quiescent and remodeling blood and lymphatic vessels in mouse airways and skin. *Arterioscler Thromb Vasc Biol.* 2007;27(3): 564–570.
29. He Y, Rajantie I, Pajusola K, et al. Vascular endothelial cell growth factor receptor 3-mediated activation of lymphatic endothelium is crucial for tumor cell entry and spread via lymphatic vessels. *Cancer Res.* 2005;65(11):4739–4746.
30. Saharinen P, Eklund L, Miettinen J, et al. Angiopoietins assemble distinct Tie2 signalling complexes in endothelial cell-cell and cell-matrix contacts. *Nat Cell Biol.* 2008;10(5):527–537.
31. Khodarev NN, Yu J, Labay E, et al. Tumour-endothelium interactions in co-culture: coordinated changes of gene expression profiles and phenotypic properties of endothelial cells. *J Cell Sci.* 2003;116(pt 6): 1013–1022.
32. Dumont DJ, Yamaguchi TP, Conlon RA, Rossant J, Breitman ML. *tek*, a novel tyrosine kinase gene located on mouse chromosome 4, is expressed in endothelial cells and their presumptive precursors. *Oncogene.* 1992;7(8):1471–1480.
33. Kozak M. An analysis of 5`-noncoding sequences from 699 vertebrate messenger RNA. *Nucleic Acids Res.* 1987;15(20):8125–8135.
34. Paterna JC, Moccetti T, Mura A, Feldon J, Bueler H. Influence of promoter and WHV post-transcriptional regulatory element on AAV-mediated transgene expression in the rat brain. *Gene Ther.* 2000;7(15):1304–1311.
35. Anisimov A, Alitalo A, Korpisalo P, et al. Activated forms of VEGF-C and VEGF-D provide improved vascular function in skeletal muscle. *Circ Res.* 2009;104(11):1302–1312.
36. Gao GP, Alvira MR, Wang L, Calcedo R, Johnston J, Wilson JM. Novel adeno-associated viruses from rhesus monkeys as vectors for human gene therapy. *Proc Natl Acad Sci U S A.* 2002;99(18):11854–11859.
37. Lin P, Buxton JA, Acheson A, et al. Antiangiogenic gene therapy targeting the endothelium-specific receptor tyrosine kinase Tie2. *Proc Natl Acad Sci U S A.* 1998;95(15):8829–8834.
38. Fukuhara S, Sako K, Minami T, et al. Differential function of Tie2 at cell-cell contacts and cell-substratum contacts regulated by angiopoietin-1. *Nat Cell Biol.* 2008;10(5):513–526.
39. Veikkola T, Lohela M, Ikenberg K, et al. Intrinsic versus microenvironmental regulation of lymphatic endothelial cell phenotype and function. *FASEB J.* 2003;17(14):2006–2013.
40. Huang Y, Song N, Ding Y, et al. Pulmonary vascular destabilization in the premetastatic phase facilitates lung metastasis. *Cancer Res.* 2009;69(19): 7529–7537.
41. Hashizume H, Falcón BL, Kuroda T, et al. Complementary actions of inhibitors of angiopoietin-2 and VEGF on tumor angiogenesis and growth. *Cancer Res.* 2010;70(6):2213–2223.

42. Daly C, Pasnikowski E, Burova E, et al. Angiopoietin-2 functions as an autocrine protective factor in stressed endothelial cells. *Proc Natl Acad Sci U S A.* 2006;103(42):15491–15496.
43. Li X, Stankovic M, Bonder CS, et al. Basal and angiopoietin-1-mediated endothelial permeability is regulated by sphingosine kinase-1. *Blood.* 2008;111(7):3489–3497.
44. Huang RL, Teo Z, Chong HC, et al. ANGPTL4 modulates vascular junction integrity by integrin signaling and disruption of intercellular VE-cadherin and claudin-5 clusters. *Blood.* 2011;118(14):3990–4002.
45. Coffelt SB, Chen YY, Muthana M, et al. Angiopoietin 2 stimulates TIE2-expressing monocytes to suppress T cell activation and to promote regulatory T cell expansion. *J Immunol.* 2011;186(7):4183–4190.
46. Mazzieri R, Pucci F, Moi D, et al. Targeting the ANG2/TIE2 axis inhibits tumor growth and metastasis by impairing angiogenesis and disabling rebounds of proangiogenic myeloid cells. *Cancer Cell.* 2011;19(4):512–526.
47. Holash J, Maisonpierre PC, Compton D, et al. Vessel cooption, regression, and growth in tumors mediated by angiopoietins and VEGF. *Science.* 1999;284(5422):1994–1998.
48. Reiss Y, Knedla A, Tal AO, et al. Switching of vascular phenotypes within a murine breast cancer model induced by angiopoietin-2. *J Pathol.* 2009;217(4):571–580.
49. Pàez-Ribes M, Allen E, Hudock J et al. Antiangiogenic therapy elicits malignant progression of tumors to increased local invasion and distant metastasis. *Cancer Cell.* 2009;15(3):220–231.

Funding

This study was supported by a research grant from MedImmune, and research grants from the Sigrid Juselius Foundation, the Finnish Cancer Organizations, the EU Microenvimet network, and the Academy of Finland (130446 to P.S., 136880 to L.E., 124127 and 140723 to K.A.). T.H. has been supported by personal grants from Finska Läkaresällskapet, K. Albin Johansson's Foundation, the Rauha and Jalmari Ahokas Foundation, and the Ida Montin Foundation. Those who provided funding did not have any involvement in the design of the study; the collection, analysis, and interpretation of the data; the writing of the article; or the decision to submit the article for publication.

Notes

C. C. Leow holds stock in AstraZeneca and is an employee of MedImmune, a subsidiary of AstraZeneca.

We acknowledge Dr Pirjo Laakkonen and Dr Caroline A. Heckman for professional help and comments on the article and Krista Heinolainen, Katja Salo, Kirsi Mänttäri, Tapio Tainola, the Biomedicum Helsinki Imaging Unit, Biocenter Finland, AAV Gene Transfer and Cell Therapy Core Facility of University of Helsinki, and the Biocenter Oulu Electron Microscopy Core Facility for their excellent technical assistance.

Affiliations of authors: Molecular/Cancer Biology Program, Research Programs Unit, Biomedicum Helsinki, University of Helsinki, Helsinki, Finland (TH, PS, GD'A, AL, AA, GZ, HH, KA); Formerly of Molecular/Cancer Biology Program, Research Programs Unit, Biomedicum Helsinki, University of Helsinki, Helsinki, Finland (ML, TT); Department of Anatomy, University of California, San Francisco, CA (ML); The Koch Institute for Integrative Cancer Research, Massachusetts Institute of Technology, Cambridge, MA (TT); Institute for Molecular Medicine Finland and Helsinki University Central Hospital, University of Helsinki, Helsinki, Finland (TH, GD'A, AA, GZ, HH, TT); Department of Medical Biochemistry and Molecular Biology, Oulu Center for Cell-Matrix Research, Biocenter Oulu, University of Oulu, Oulu, Finland (LE); Biocenter Oulu, Department of Pathology, University of Oulu, Oulu, Finland (RS); Department of Pathology, Beth Israel Deaconess Medical Center, Harvard Medical School, Boston, MA (LEB); Department of Molecular Medicine, A.I. Virtanen Institute, University of, Eastern Finland, Kuopio, Finland (SY-H); Department of Pre-Clinical Oncology, MedImmune, Gaithersburg, MD (CCL); Biomedical Research Center and Department of Biological Sciences, Korea Advanced Institute of Science and Technology, Daejeon, Korea (GYK).